Spatial coherence of the insulating phase in quasi-two-dimensional LaNiO3 films

著者	Masato Anada, Kazuhiro Kowa, Hiroki Maeda, Enju Sakai, Miho Kitamura, Hiroshi Kumigashira, Osami Sakata, Yoshinori Nakanishi-Ohno, Masato Okada, Tsuyoshi Kimura, Yusuke Wakabayashi
journal or publication title	Physical Review B
volume	98
number	014105
page range	1-8
year	2018-07-10
URL	http://hdl.handle.net/10097/00125558

doi: 10.1103/PhysRevB.98.014105

Spatial coherence of the insulating phase in quasi-two-dimensional $LaNiO_3$ films

Masato Anada,[1] Kazuhiro Kowa,[1] Hiroki Maeda,[1] Enju Sakai,[2,*] Miho Kitamura,[2] Hiroshi Kumigashira,[2,3] Osami Sakata,[4] Yoshinori Nakanishi-Ohno,[5,6] Masato Okada,[7] Tsuyoshi Kimura,[1,7] and Yusuke Wakabayashi[1,†]

[1]*Division of Materials Physics, Graduate School of Engineering Science, Osaka University, Toyonaka 560-8531, Japan*
[2]*Institute of Materials Structure Science, High Energy Accelerator Research Organization, Tsukuba, Ibaraki 305-0801, Japan*
[3]*Institute of Multidisciplinary Research for Advanced Materials, Tohoku University, Sendai 980-8577, Japan*
[4]*Synchrotron X-ray Station at SPring-8, National Institute for Materials Science (NIMS), Sayo 679-5148, Japan*
[5]*Graduate School of Arts and Sciences, The University of Tokyo, Meguro, Tokyo 153-8902, Japan*
[6]*Precursory Research for Embryonic Science and Technology (PRESTO), Japan Science and Technology Agency, Kawaguchi, Saitama 332-0012, Japan*
[7]*Graduate School of Frontier Sciences, The University of Tokyo, Kashiwa, Chiba 277-8561, Japan*

(Received 29 March 2018; revised manuscript received 19 June 2018; published 10 July 2018)

The quasi-two-dimensional nature of $LaNiO_3$ (LNO) thin films on $SrTiO_3$(001) (STO) and $LaAlO_3$(001) (LAO) substrates is examined. Although both samples undergo a metal-insulator transition with decreasing thickness, the spatial distributions of the insulating phase within the films differ from each other. The LNO cell volume of the insulating phase in LNO/STO is larger than that of the metallic phase, and the large cells remain at the interface in thick films with metallic conduction, suggesting a high oxygen-vacancy content at the interface. The cell volume of the insulating phase in LNO/LAO is smaller than that of the metallic phase, and the cell volume of the entire film changes coherently. The cell-volume decrease indicates that the bonding changes from bulklike to covalent.

DOI: 10.1103/PhysRevB.98.014105

I. INTRODUCTION

Epitaxial interfaces of perovskite oxides provide us with an opportunity to study the effect of low dimensionality on strongly correlated electron systems. Because electrons are affected by surrounding electrons, their behavior must be different at surfaces [1–3] or interfaces [4–7], where they have no or different neighbors, compared with that in the bulk material. The RNiO$_3$ thin-film system (R: rare-earth ion) is an archetypal strongly correlated d-electron system in the charge transfer regime [8–10]. Many studies have shown that $LaNiO_3$ (LNO) films behave, like their bulk counterpart [11], as a paramagnetic metal when they are thick enough. However, when LNO films are thinner than two [12,13] to five [14] unit cells (u.c.) thick, the films show insulating behavior under both compressive and tensile strains [14–16], as shown in Fig. 1(a). The insulating behavior of LNO thin films has been rationalized based on the dimensionality of carrier conduction [14,17]. Many mechanisms for the thickness-dependent metal-insulator transition of LNO thin films have been proposed, such as disorder-driven localization [14], the rotation of NiO_6 octahedra [18], and strain induced by the substrate [19].

Various phenomena observed at oxide interfaces are caused by the complex effects of epitaxial strain, quantum confinement, interfacial charge transfer, degree of p-d hybridization, and uncontrollable interfacial chemical perturbation. Spectroscopic measurements can provide information about the charge transfer and modulation of the band structure at a material interface and therefore are widely used in film studies [12,17,20,21]. The photoemission spectra of LNO grown on Nb-doped $SrTiO_3$ (Nb:STO) and $LaAlO_3$ (LAO) [20] are presented in Figs. 1(b) and 1(c), respectively. As expected from the macroscopic conductivity of these samples, the density of states around the Fermi energy E_F depended on the LNO film thickness. In both cases, no density of states was found at E_F in the films that were less than ∼3 u.c. thick, which agrees with the transport property presented in Fig. 1(a). What was not expected were the different thickness variations of the leading edge of the valence-band spectra of LNO grown on STO [21] and LAO [20]. The sample grown on STO shows a large jump in its density of states when the fourth LNO layer is grown, while the change in the density of states of the LNO films on LAO appears to be much more gradual. This difference implies that the origin of the insulating states in these two film systems is different. To obtain a better understanding of this difference, experimental observation from a different viewpoint is needed.

One of the complementary techniques to spectroscopy is diffraction. Structural information can provide direct knowledge of the chemical perturbation or spatial coherency of electronic states. However, there have been few structural studies of nickelate ultrathin films [16,22–24]. In this study, the different insulating states in LNO/STO and LNO/LAO systems are examined through a systematic interfacial structure study of the thickness range covering the metal-insulator transition. As a result, it is clarified that the insulating nature of LNO on STO is induced by oxygen vacancies, whereas that of LNO on LAO is caused by the coherent change in the bonding nature.

*Present address: Environmental Science Center, The University of Tokyo, Hongo 7-3-1, Bunkyo-ku, Tokyo 113-0033, Japan.
†wakabayashi@mp.es.osaka-u.ac.jp

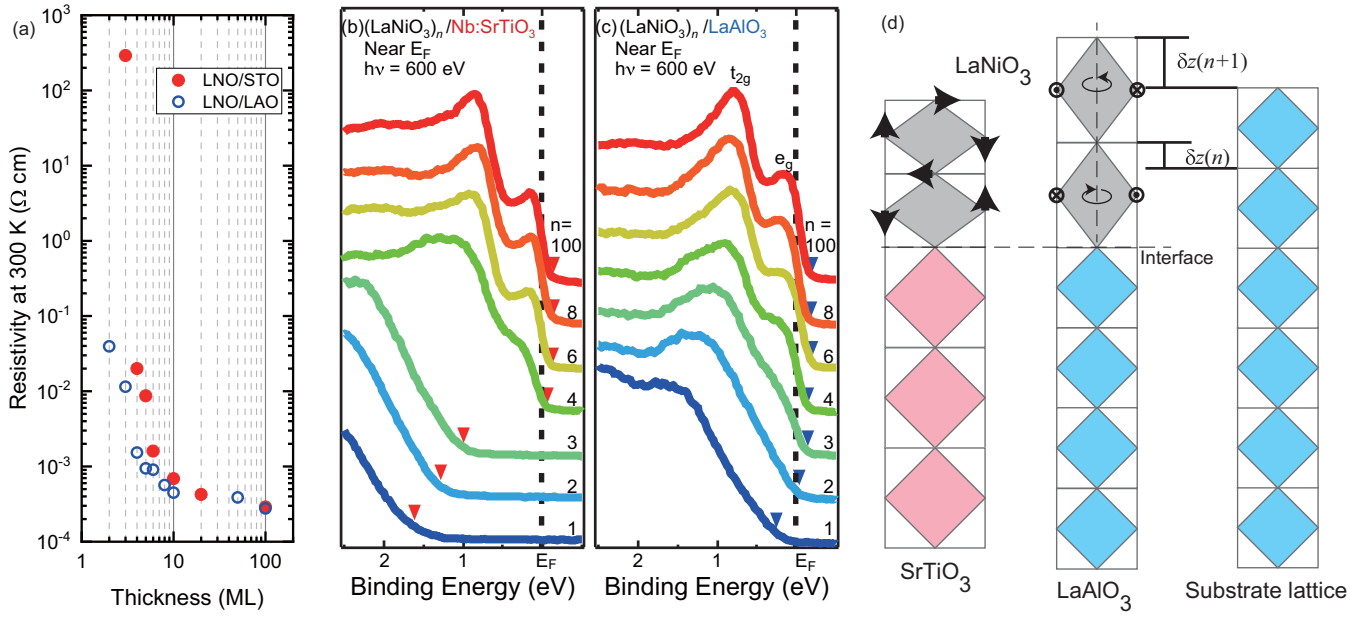

FIG. 1. (a) Thickness dependence of the electric resistivity. (b),(c) Photoelectron spectra of LNO/Nb:STO and LNO/LAO [20], respectively. Triangles show the leading-edge energy. (d) Schematics of LNO/STO and LNO/LAO interfacial structures. The octahedral rotations in LNO thick films on STO and LAO reported in Ref. [25] are also shown.

Here we summarize the known structural information of LNO thick films. For the LNO films on STO, the NiO_6 octahedra tilt from the c direction (the surface normal direction), whereas octahedral rotation within the c plane was observed for the LNO films on LAO [25], as shown in Fig. 1(d). The c-lattice parameter of LNO on STO is 3.801 ± 0.006 Å [25,26] and that on LAO is 3.901 ± 0.006 Å [20,25]. The c-lattice parameter of LNO on STO was increased by 0.05 Å when the oxygen partial pressure during film growth was decreased from 0.2 to 0.02 mbar [26], which is a result of the introduction of oxygen vacancies. As for the known structural information of LNO ultrathin films, there have been several reports on samples grown by molecular beam epitaxy (MBE) [16,22–24]. Local polarization estimated by relative displacement of oxygen and metal sites was reported for an LNO film with a thickness of 4 u.c. [22]. Cation displacement from the oxygen layer by ~0.1 Å was found to occur only a few u.c. from the surface, in accordance with their theoretical calculation. Termination layer dependence has been studied for LaO-terminated 3 and 4 u.c. LNO films and an NiO_2-terminated 3.5 u.c. LNO film deposited on top of an LAO (001) surface [23]. The LaO-terminated films were metallic and the polarization was limited to the very surface layer. This structure was quite different from that of the NiO_2-terminated insulating film, which showed local polarization as deep as 10 Å from the surface. Such difference in properties controlled by the termination layer is not surprising because the (001) surfaces of LAO and LNO are polar, so changing the termination layer reversed the local electric field. The effect of an LAO cap layer on top of LNO/LAO films was reported in Ref. [24]. The Ni-O-Ni bond angle, which is related to the transfer integral, was strongly affected by the cap layer. In this study, we measured the dependence of the structure of LNO thin films grown on STO and LAO (001) surfaces on LNO thickness.

II. EXPERIMENT

LNO thin films with a thickness of n u.c. were grown on atomically flat (001) surfaces of Nb:STO ($n = 2$ to 5) and LAO ($n = 1$ to 5) by pulsed laser deposition (PLD); we denote these samples as $(LNO)_n$/STO and $(LNO)_n$/LAO, respectively. During deposition, the substrate temperature was maintained at 450 °C under an oxygen pressure of 10^{-3} torr. The film thickness was precisely controlled on the atomic scale by monitoring the intensity oscillation of reflection high-energy electron diffraction. The films were subsequently annealed at 400 °C for 45 min under oxygen at atmospheric pressure to fill the residual oxygen vacancies. The LNO/STO samples were prepared just before the synchrotron measurements because storage at room temperature induces oxygen-vacancy formation [27]. No such sample degradation was found for the LNO/LAO samples.

The transport properties of the LNO films presented in Fig. 1 were measured by the four-probe technique. Nondoped STO substrates were used for these measurements. Temperature variation of the resistivity of $(LNO)_n$/STO for $n \geqslant 4$ is similar to the reported ones [16]. That for $(LNO)_n$/LAO has already been reported in Ref. [20].

The photoemission spectra presented in Fig. 1 were measured *in situ* at BL-2C of the Photon Factory, KEK, Japan [20]. The spectra were recorded using a Scienta SES-2002 electron energy analyzer with a total-energy resolution of 120 meV at a photon energy of 600 eV. The Fermi level of the samples was calibrated using gold foil as a reference. The x-ray absorption spectroscopy (XAS) spectra were also acquired *in situ* by measuring the sample drain current.

The crystal truncation rod (CTR) scattering measurements were performed with the four-circle diffractometers installed at BL-3A and BL-4C at the Photon Factory, KEK, Japan and BL15XU of SPring-8, Japan. The x-ray energy was 12.0 or

12.4 keV, which are both nonresonant conditions. The typical beam size was 0.5 × 0.5 mm. During the measurements, the samples were kept in a vacuum chamber at 10^{-5} torr or Kapton dome filled with He gas to avoid possible radiation damage. The scattering intensity from LNO/LAO samples was detected by a two-dimensional pixel array detector XPAD (imXpad), and that from LNO/STO samples was detected by an ordinary point detector. Illumination area and Lorentz factor corrections were applied following the formula provided in Ref. [28]. For all samples except for $(LNO)_4$/STO, the 00, 01, 02, 11, and 12 rods were measured up to at least $l = 4.0$. The data for the 11 and 12 rods were missing for $(LNO)_4$/STO. Structure refinement and estimation of the standard deviations of parameters were performed using the maximum *a posteriori* estimation described in Ref. [29]. The prior probability of film thickness for each n u.c. sample was assumed to be a Gaussian distribution with an average and standard deviation of n and $0.1 \times n$, respectively. In this study, in-plane atomic displacement was neglected; i.e., only the occupancy parameters and out-of-plane atomic displacements were refined. Atomic displacement parameters, which reflect the amplitude of the thermal vibration, were fixed to $B = 0.4$ Å^2 to reduce the number of parameters.

III. RESULTS AND ANALYSIS

A. X-ray absorption spectroscopy

Ni-2p XAS spectra for LNO/STO and LNO/LAO are presented in Fig. 2. Here, we focus on the Ni-2p XAS spectra at the Ni-L_2 edge because the (Ni-L_3)-edge structure partially overlaps with the very strong La-M_4 absorption edge owing to the close proximity of the two energy levels [30,31]. In order to examine the valence of Ni ions in the thin films, the energy of Ni^{3+} (871.9 eV) and Ni^{2+} (870.3 eV) signals in perovskite nickelates [32] are indicated by solid lines. As can be seen in Fig. 2, the Ni^{2+} signal is seen only in $(LNO)_n$/STO with small n values; $(LNO)_2$/STO exhibits a prominent doublet structure, which is characteristic of an Ni^{2+} state [32]. With increasing n, the doublet structure of the Ni-L_2 edge around 871 eV gradually smears and eventually changes into a broad single-peak structure of Ni^{3+} states. In contrast, $(LNO)_n$/LAO do not show an obvious indication of Ni^{2+} states. Although the precise spatial distribution of the Ni^{2+} states in the LNO films was unclear from this measurement, these results strongly suggest that the Ni^{2+} states are generated at the initial stage of LNO film growth on STO.

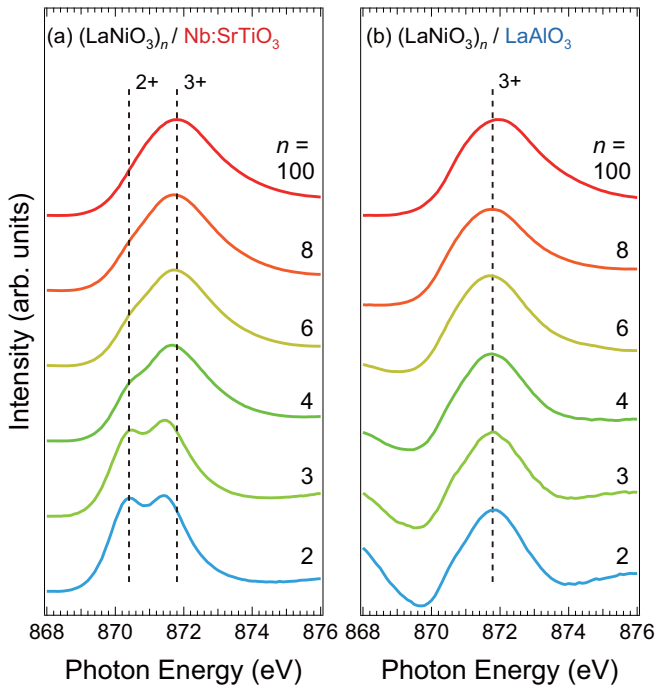

FIG. 2. Ni $2p_{1/2}$ XAS spectra for (a) $(LNO)_n$/Nb:STO and (b) $(LNO)_n$/LAO ($n = 2$ to 100).

B. CTR scattering

CTR scattering data along the 00 rod measured for the LNO films on STO and LAO substrates are presented in Fig. 3. The number of bumps between the substrate Bragg peaks increased with n, as expected from a simple calculation of interference. However, unlike the bulk structure determination, the lattice spacing of the film could not be derived from the peak positions. This is because the lattice spacing for the ith layer from the surface is not necessarily the same as that of the $(i + 1)$th layer. In addition, the "Bragg reflections" for ultrathin films are ill defined; one cannot find clear Bragg peak positions for the films. Therefore, one has to perform a structure refinement using the CTR profiles even to derive the lattice spacing as a function of the depth. The solid curves in Fig. 3 show the calculated intensity derived from the refined structure. The typical value of $R \equiv \sum |(|F_{\rm expt}| - |F_{\rm calc}|)| / \sum |F_{\rm expt}|$ is 0.2, where $F_{\rm expt}$ and $F_{\rm calc}$ denote the square root of the measured intensity and calculated intensity, respectively. Although the structure parameters of oxygen are rather unreliable, those determined for heavy elements stably converged regardless of the details of the fitting procedure and constraints applied.

Figure 4 shows the depth profiles of La occupancy and A-site atomic displacement δz with respect to the substrate lattice, which is illustrated in Fig. 1(d). The lattice spacing is defined by the slope of the curve of δz. Deep inside the substrate, the slope is zero by definition. The thick solid lines are the slopes for the lattice parameter of thick films on STO [25,26] and LAO [20,25] substrates. The slopes for the thick films coincide with the slopes determined for $(LNO)_5$/STO and $(LNO)_5$/LAO.

For the films on STO substrates, the change in the lattice spacing of the LNO film from that of the substrate around their interface is small. The change starts around the third layer from the nominal interface ($z = 0$ position in Fig. 4). The $n = 2$ and 3 films have almost the same spacing as that of STO, and the following layers in thicker films have smaller lattice spacings. The $n = 5$ film has a lattice spacing close to that of a thick LNO film [25,26] of 3.80 Å only in the layers furthest away from the LNO/STO interface. Therefore, the lattice spacing of the LNO films is strongly affected by the substrate within the range of ∼3 u.c. from the interface.

For the LNO films on LAO substrates, two trends in the depth profiles of the A-site atomic displacements are visible. The metallic samples, $n = 4$ and 5, have a larger lattice spacing than that of the insulating samples, $n \leqslant 3$. The lattice spacing

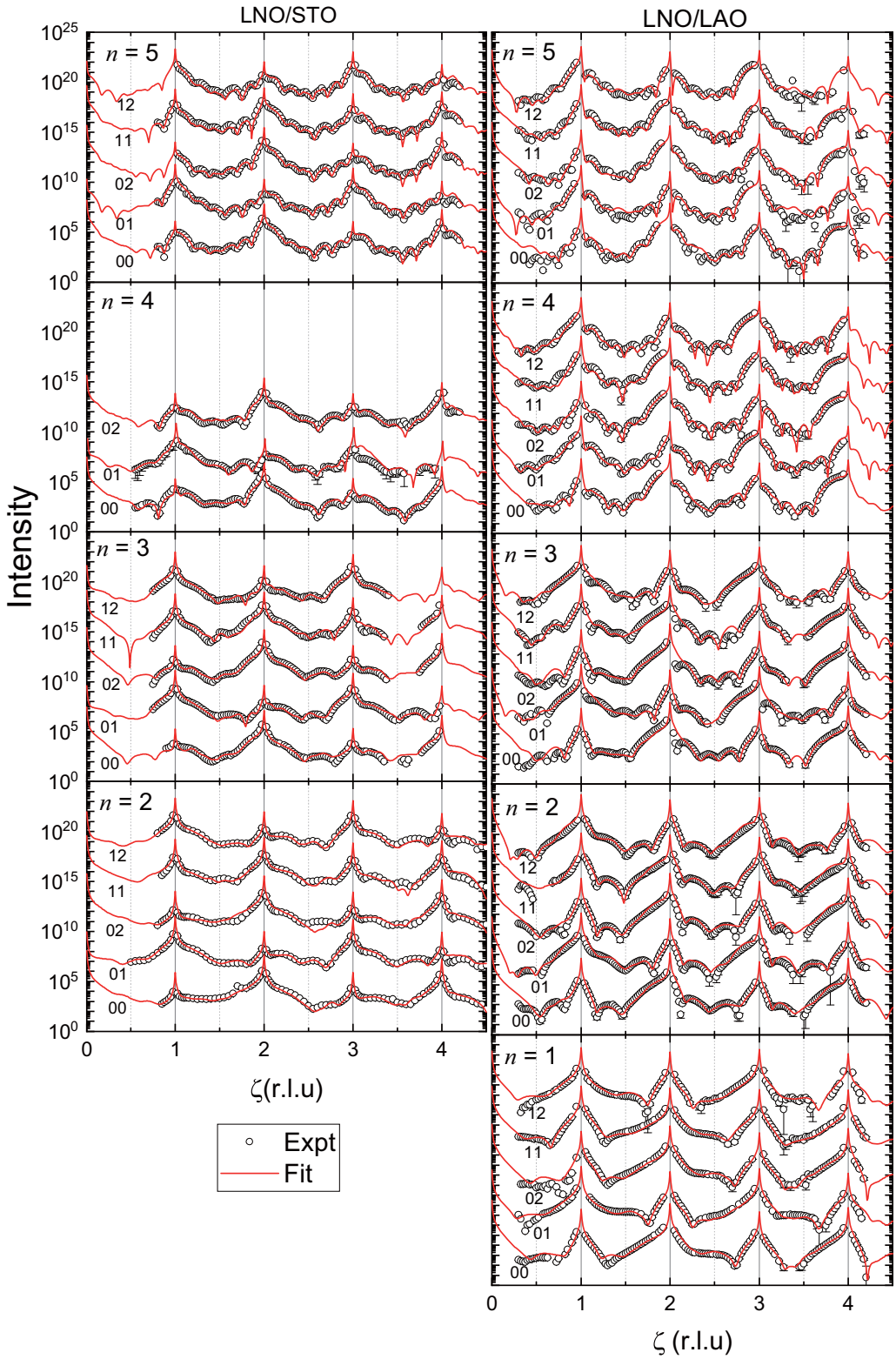

FIG. 3. CTR scattering profiles along the $hk\zeta$ rods for $(LNO)_n/STO$ ($n = 2$ to 5) (left) and $(LNO)_n/LAO$ ($n = 1$ to 5) (right). Open symbols show the experimental results, and the solid curves show the calculated intensity derived from the refined structure. The error bars, which are shorter than the symbol size for most of the plots, show the statistical error.

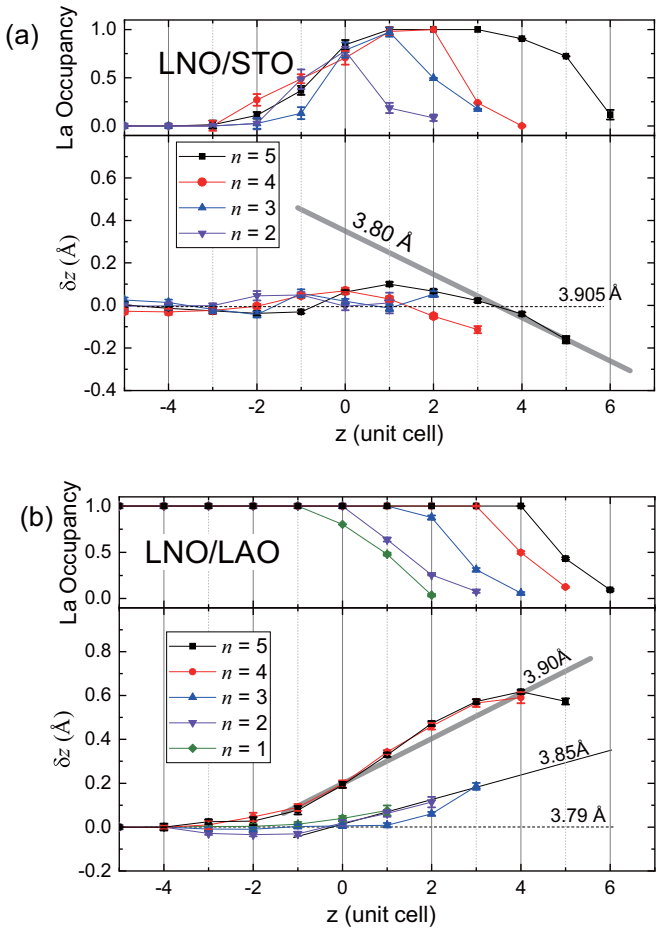

FIG. 4. (a) *A*-site atomic displacement from the $SrTiO_3$ substrate lattice as a function of depth. The origin of the horizontal axis is defined as the nominal interface and that of the vertical axis is defined as the substrate lattice. The lattice parameter reported for thick films [25,26] is shown as a thick solid line. The depth dependence of La occupancy is also shown in the top panel. (b) *A*-site atomic displacement from the $LaAlO_3$ substrate lattice as a function of depth. The lattice parameter reported for thick films [20,25] is shown as a thick solid line.

of the $n = 4$ and 5 samples is the same as that of an $n = 100$ sample, i.e., 3.90 Å, that displays metallic conductivity [20]. The "dead layer" seen at LNO/STO interfaces is absent in LNO/LAO interfaces.

IV. DISCUSSION

Our structural study clearly illustrates the difference between the insulating states of LNO/STO and LNO/LAO. The metal-insulator transition in the LNO/LAO system occurred coherently. Because the thickness controls the electronic state of the entire LNO film, the transition is triggered by the dimensionality. In contrast, the insulating phase found in the present LNO/STO samples appears to be caused by chemical reasons rather than dimensionality. The remaining issue is the difference between the electronic states of the metallic and insulating phases.

A. LNO/STO interface

Let us examine the LNO/STO interface first. While the LNO/STO interface involves La-Sr atomic interdiffusion, which is exhibited in Fig. 4(a), it should not play an important role in the metal-insulator transition. The reason is that the transition is reported in the samples having a different degree of interfacial mixing, i.e., the samples made by MBE [16], rf magnetron sputtering [14], and PLD (this work). In particular, Ref. [16] reports the depth profile of the electron density, showing smaller atomic interdiffusion at the interface than our sample.

The $n = 2$ and 3 samples have a lattice spacing of ~3.905 Å, which is 0.1 Å longer than that of the thick films. Such elongation can be caused by (i) valence modulation of Ni by electrostatic doping, (ii) change in the NiO_6 octahedral tilting, or (iii) introduction of oxygen vacancies.

Because a Ni^{2+} ion is larger than a Ni^{3+} one, introducing Ni^{2+} expands the lattice spacing of LNO. According to the bond valence sum method, the expected Ni^{2+}-O distance is 4% longer than the Ni^{3+}-O distance. The interfacial expansion of the LNO lattice spacing for 2- and 3-u.c.-thick samples is 3%. Therefore, to account for the lattice expansion caused by introducing Ni^{2+}, 70% to 80% of Ni sites should be occupied by Ni^{2+}. The amount of carrier modulation induced by the electrostatic doping mechanism estimated based on the Thomas-Fermi screening length and dielectric constant is less than 10% [21]. Therefore, electrostatic doping cannot account for the observed lattice expansion.

The octahedral tilting is affected by the connectivity to the substrate, and the octahedral tilt angle changes gradually from the value of the substrate to that of the film within 5 u.c. of the epitaxial interface [18,33,34]. For the LNO/STO samples, STO has no octahedral tilting in its bulk form. If the first 2 to 3 u.c. of LNO keeps the small octahedral tilting, we should expect larger lattice spacing than that of ordinary LNO. The expected maximum lattice spacing is twice the apical Ni-O distance. However, the lattice spacing of 3.905 Å found for the $n = 2$ and 3 samples is longer than twice the reported Ni-O distance (3.866 Å [25]).

Another way to expand the lattice spacing is oxygen vacancies. An LNO film on an STO substrate suffers from the thermal escape of oxygen atoms even at room temperature [27], which suggests that oxygen has a very low binding energy around the LNO/STO interface. Recent *ab initio* calculation also predicts the oxygen-vacancy formation at the LNO/STO interface [16]. Oxygen vacancies introduce Ni^{2+}, which makes the lattice expand, in addition to the expansion caused by the Coulomb repulsion between cations. The above-mentioned 70% to 80% of Ni^{2+} is achieved when the interfacial composition is $LaNiO_{2.60}$ to $LaNiO_{2.65}$. Such an amount of Ni^{2+} localized at the interface well explains the XAS result presented in Fig. 2. As a result, we have achieved the interface structure schematically illustrated in Fig. 5(a). Reference [16], which reports a result of 00ζ-CTR measurement on MBE-made LNO/STO interface, also reached the interfacial oxygen-vacancy formation.

Oxygen vacancies also alter the local potential distribution and give rise to a wide band gap at E_F [16,35,36]. Therefore, we conclude that there is a large amount of oxygen vacancies at the interface, and the oxygen deficiency causes the insulating

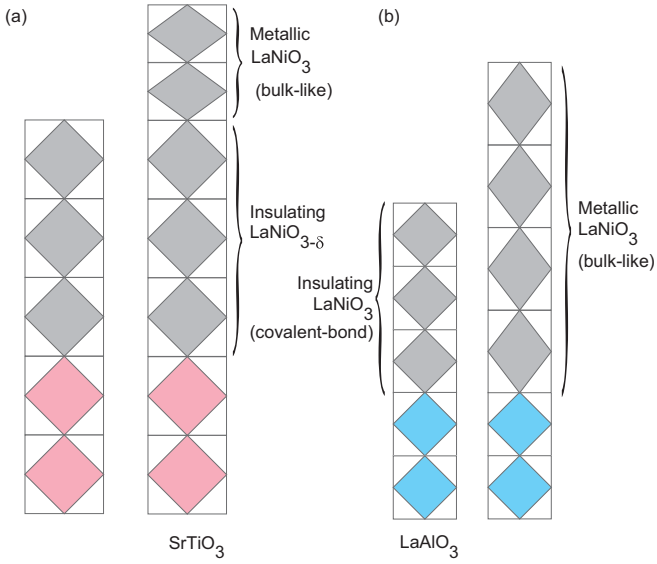

FIG. 5. (a) Schematic of LNO/STO interfacial structure. (b) That of LNO/LAO interfacial structure.

nature of $(LNO)_n$/STO for $n \leqslant 3$. This interpretation is in accordance with the photoemission spectroscopy results indicating the formation of insulating LNO layers at the interface with Nb:STO [21], although the insulating layer was attributed to the formation of a Schottky barrier in that study.

B. LNO/LAO interface

The LNO/LAO samples clearly show a change in the electronic structure of the entire film when the fourth layer is deposited. There are several ways to make LNO insulating, but many of them can be easily excluded. Here, we examine the Jahn-Teller (JT) effect, charge disproportionation, surface termination, and covalent bond–ionic bond crossover.

One of the common origins of octahedral distortion in perovskite oxides is the JT effect. Ni^{3+} in the ionic limit has the e_g^1 configuration, which is JT active. Therefore, an orbital order-driven insulating state appears to be a natural consequence. However, the distortion of the lattice parameter measured by the c/a value in the insulating state is closer to unity than that in the metallic state, which contradicts the formation of a JT-driven insulating state. The lack of JT distortion is caused by the hybridization of the oxygen p band and Ni d band [7,37].

Although charge disproportionation has been reported for many bulk nickelates [38–40], the results of XAS presented in Fig. 2(b) and Ref. [20] excluded the possibility of charge disproportionation.

Surface termination is known to affect conductivity [23]. However, no clear difference in surface termination was found for the metallic and insulating LNO films in our analysis.

Nickelates have close Ni $3d$ and oxygen $2p$ energy levels, leading to the idea of a covalent insulator [10,41], which is a charge transfer insulator with a negative effective energy gap between the upper Hubbard band and oxygen p-band Δ. In other words, the upper Hubbard band and oxygen p band overlap in many nickelates. To make LNO an insulator, a sizable amount of hybridization to form covalent bonds is needed. The metallic and covalent bond lengths of Ni-O bonds are 1.938 ± 0.004 and 1.918 ± 0.006 Å, respectively [42]. When we assume the Ni-O bond is normal to the surface, the c-lattice spacings calculated for metallic and insulating states are 3.88 and 3.84 Å, respectively. The measured c-lattice spacings for metallic and insulating LNO/LAO are 3.91 and 3.85 Å, respectively, which agree well with the metallic and covalent bond lengths. Note that the out-of-plane Ni-O-Ni bond angle in an LNO thick film on LAO is $175.2^\circ \pm 0.6^\circ$ [25], which supports the assumption we made for this discussion. As a result, we conclude the interface structure illustrated in Fig. 5(b).

The binding energy of the t_{2g} electrons is increased in the insulating phase, as shown in Fig. 1(c). This feature may be interpreted to an increase of the energy splitting of e_g and t_{2g} levels through the decrease of the Ni-O bond length caused by the formation of covalent bonds at the first approximation. Such an increase in the t_{2g} binding energy has been interpreted from the similarity with the spectra observed in the charge ordering of $NdNiO_3$ [12], although the complicated energy shift due to band alignment between the two oxides is also considered in the present heterostructures [21]. It should be noted that the crystal field is based on the ionic picture, which is, strictly speaking, irrelevant to this case. The number of electron for each Ni is unchanged by the metal-insulator transition. The electronic configuration is $t^6\sigma^*$. The p-d transfer integral determines if the band gap opens to the σ^* band [41].

V. CONCLUSION

The lattice spacings of LNO thin films on STO and LAO substrates were examined as a function of LNO film thickness using surface x-ray diffraction. The results clearly showed the difference in the spatial coherence of the insulating phase in LNO/STO and LNO/LAO. The insulating phase in LNO/STO was caused by oxygen deficiency and stayed at the interface even when the film was thicker than 4 u.c. In contrast, the insulating phase in LNO/LAO was stabilized by the low dimensionality. When the LNO film got thicker than 4 u.c., the whole film became metallic. The insulating LNO had a bond length corresponding to the covalent bond, whereas the metallic phase had the bond length expected for metallic nickel oxides. The insulator-metal transition observed for LNO/LAO was therefore the transition from a covalent crystal to ordinary bulklike LNO. This structural study revealed the importance of the systematic examination of interfacial structure to conceive a relevant effective model of interfacial electronic structure because interfacial electronic structure can be modulated by phenomena such as atomic intermixing and unintentional vacancy introduction, as well as by often discussed purely electronic interactions.

ACKNOWLEDGMENTS

We thank Prof. Y. Morikawa and Dr. H. D. Nguyen for fruitful discussion. This work was supported by a Grant-in-Aid for Scientific Research [Japan Society for the Promotion of Science (JSPS) KAKENHI, Grants No. JP16H02115 and No. JP26105008] and by Japan Science and Technology Agency (JST), PRESTO (Grant No. JPMJPR1773). The synchrotron

radiation experiments at the Photon Factory were performed with the approval of the Photon Factory Program Advisory Committee (Proposals No. 2012G091, No. 2013S2-002, No. 2015S2-005, and No. 2015S2-009). The synchrotron diffraction measurements at SPring-8 were performed at the NIMS Synchrotron X-ray Station under Proposals No. 2012B4901 and No. 2013A4901 as part of the NIMS Nanotechnology Platform (Projects No. A-12-NM-0030 and No. A-13-NM-0002).

[1] J. W. Freeland, K. E. Gray, L. Ozyuzer, P. Berghuis, E. Badica, J. Kavich, H. Zheng, and J. F. Mitchell, Full bulk spin polarization and intrinsic tunnel barriers at the surface of layered manganites, Nat. Mater. **4**, 62 (2005).

[2] Y. Wakabayashi, M. H. Upton, S. Grenier, J. P. Hill, C. S. Nelson, J.-W. Kim, P. J. Ryan, A. I. Goldman, H. Zheng, and J. F. Mitchell, Surface effects on the orbital order in the single-layered manganite $La_{0.5}Sr_{1.5}MnO_4$, Nat. Mater. **6**, 972 (2007).

[3] Y. Yamasaki, J. Fujioka, H. Nakao, J. Okamoto, T. Sudayama, Y. Murakami, M. Nakamura, M. Kawasaki, T. Arima, and Y. Tokura, Surface ordering of orbitals at a higher temperature in $LaCoO_3$ thin film, J. Phys. Soc. Jpn. **85**, 023704 (2016).

[4] A. Ohtomo, D. A. Muller, J. L. Grazul, and H. Y. Hwang, Artificial charge-modulation in atomic-scale perovskite titanate superlattices, Nature (London) **419**, 378 (2002).

[5] Ş. Smadici, P. Abbamonte, A. Bhattacharya, X. Zhai, B. Jiang, A. Rusydi, J. N. Eckstein, S. D. Bader, and J.-M. Zuo, Electronic Reconstruction at $SrMnO_3$-$LaMnO_3$ Superlattice Interfaces, Phys. Rev. Lett. **99**, 196404 (2007).

[6] M. Nakamura, D. Okuyama, J. S. Lee, T.-h. Arima, Y. Wakabayashi, R. Kumai, M. Kawasaki, and Y. Tokura, Magnetically tunable metal-insulator superlattices, Adv. Mater. **22**, 500 (2010).

[7] E. Benckiser, M. W. Haverkort, S. Brück, E. Goering, S. MacKe, A. Frañó, X. Yang, O. K. Andersen, G. Cristiani, H.-U. Habermeier, A. V. Boris, I. Zegkinoglou, P. Wochner, H.-J. Kim, V. Hinkov, and B. Keimer, Orbital reflectometry of oxide heterostructures, Nat. Mater. **10**, 189 (2011).

[8] J. Chaloupka and G. Khaliullin, Orbital Order and Possible Superconductivity in $LaNiO_3$/$LaMO_3$ Superlattices, Phys. Rev. Lett. **100**, 016404 (2008).

[9] A. S. Disa, F. J. Walker, S. Ismail-Beigi, and C. H. Ahn, Research update: Orbital polarization in $LaNiO_3$-based heterostructures, APL Mater. **3**, 062303 (2015).

[10] S. Middey, J. Chakhalian, P. Mahadevan, J. W. Freeland, A. J. Millis, and D. D. Sarma, Physics of ultrathin films and heterostructures of rare-earth nickelates, Annu. Rev. Mater. Res. **46**, 305 (2016).

[11] M. L. Medarde, Structural, magnetic and electronic properties of $RNiO_3$ perovskites (R = rare earth), J. Phys.: Condens. Matter **9**, 1679 (1997).

[12] P. D. C. King, H. I. Wei, Y. F. Nie, M. Uchida, C. Adamo, S. Zhu, X. He, I. Božović, D. G. Schlom, and K. M. Shen, Atomic-scale control of competing electronic phases in ultrathin $LaNiO_3$, Nat. Nanotech. **9**, 443 (2014).

[13] B. Lau and A. J. Millis, Theory of the Magnetic and Metal-Insulator Transitions in $RNiO_3$ Bulk and Layered Structures, Phys. Rev. Lett. **110**, 126404 (2013).

[14] R. Scherwitzl, S. Gariglio, M. Gabay, P. Zubko, M. Gibert, and J.-M. Triscone, Metal-Insulator Transition in Ultrathin $LaNiO_3$ films, Phys. Rev. Lett. **106**, 246403 (2011).

[15] J. Son, P. Moetakef, J. M. LeBeau, D. Ouellette, L. Balents, S. J. Allen, and S. Stemmer, Low-dimensional Mott material: Transport in ultrathin epitaxial $LaNiO_3$ films, Appl. Phys. Lett. **96**, 062114 (2010).

[16] I.-C. Tung, G. Luo, J. H. Lee, S. H. Chang, J. Moyer, H. Hong, M. J. Bedzyk, H. Zhou, D. Morgan, D. D. Fong, and J. W. Freeland, Polarity-driven oxygen vacancy formation in ultrathin $LaNiO_3$ films on $SrTiO_3$, Phys. Rev. Mater. **1**, 053404 (2017).

[17] J. Liu, S. Okamoto, M. van Veenendaal, M. Kareev, B. Gray, P. Ryan, J. W. Freeland, and J. Chakhalian, Quantum confinement of Mott electrons in ultrathin $LaNiO_3$/$LaAlO_3$ superlattices, Phys. Rev. B **83**, 161102 (2011).

[18] J. Hwang, J. Son, J. Y. Zhang, A. Janotti, C. G. Van de Walle, and S. Stemmer, Structural origins of the properties of rare earth nickelate superlattices, Phys. Rev. B **87**, 060101 (2013).

[19] J. Chakhalian, J. M. Rondinelli, J. Liu, B. A. Gray, M. Kareev, E. J. Moon, N. Prasai, J. L. Cohn, M. Varela, I. C. Tung, M. J. Bedzyk, S. G. Altendorf, F. Strigari, B. Dabrowski, L. H. Tjeng, P. J. Ryan, and J. W. Freeland, Asymmetric Orbital-Lattice Interactions in Ultrathin Correlated Oxide Films, Phys. Rev. Lett. **107**, 116805 (2011).

[20] E. Sakai, M. Tamamitsu, K. Yoshimatsu, S. Okamoto, K. Horiba, M. Oshima, and H. Kumigashira, Gradual localization of Ni 3d states in $LaNiO_3$ ultrathin films induced by dimensional crossover, Phys. Rev. B **87**, 075132 (2013).

[21] H. K. Yoo, Y. J. Chang, L. Moreschini, H.-D. Kim, C. H. Sohn, S. Sinn, J. S. Oh, C.-T. Kuo, A. Bostwick, E. Rotenberg, and T. W. Noh, Insulating-layer formation of metallic $LaNiO_3$ on Nb-doped $SrTiO_3$ substrate, Appl. Phys. Lett. **106**, 121601 (2015).

[22] H. Chen, D. P. Kumah, A. S. Disa, F. J. Walker, C. H. Ahn, and S. Ismail-Beigi, Modifying the Electronic Orbitals of Nickelate Heterostructures Via Structural Distortions, Phys. Rev. Lett. **110**, 186402 (2013).

[23] D. P. Kumah, A. Malashevich, A. S. Disa, D. A. Arena, F. J. Walker, S. Ismail-Beigi, and C. H. Ahn, Effect of Surface Termination on The Electronic Properties of $LaNiO_3$ Films, Phys. Rev. Appl. **2**, 054004 (2014).

[24] D. P. Kumah, A. S. Disa, J. H. Ngai, H. Chen, A. Malashevich, J. W. Reiner, S. Ismail-Beigi, F. J. Walker, and C. H. Ahn, Tuning the structure of nickelates to achieve two-dimensional electron conduction, Adv. Mater. **26**, 1935 (2014).

[25] S. J. May, J.-W. Kim, J. M. Rondinelli, E. Karapetrova, N. A. Spaldin, A. Bhattacharya, and P. J. Ryan, Quantifying octahedral rotations in strained perovskite oxide films, Phys. Rev. B **82**, 014110 (2010).

[26] F. Sánchez, C. Ferrater, C. Guerrero, M. V. García-Cuenca, and M. Varela, High-quality epitaxial $LaNiO_3$ thin films on $SrTiO_3$(100) and $LaAlO_3$(100), Appl. Phys. A **71**, 59 (2000).

[27] Y. Wakabayashi, H. Maeda, T. Kimura, O. Sakata, E. Sakai, and H. Kumigashira, Microscopic observation of degradation of $LaNiO_3$ ultrathin films caused by air exposure, e-J. Surf. Sci. Nanotech. **14**, 14 (2016).

[28] C. M. Schlepütz, R. Herger, P. R. Willmott, B. D. Patterson, O. Bunk, Ch. Brönnimann, B. Henrich, G. Hülsen, and E. F. Eikenberry, Improved data acquisition in grazing-incidence X-ray scattering experiments using a pixel detector, Acta Crystallogr. A **61**, 418 (2005).

[29] M. Anada, Y. Nakanishi-Ohno, M. Okada, T. Kimura, and Y. Wakabayashi, Bayesian inference of metal oxide ultrathin film structure based on crystal truncation rod measurements, J. Appl. Crystallogr. **50**, 1611 (2017).

[30] J. C. Rojas Sánchez, B. Nelson-Cheeseman, M. Granada, E. Arenholz, and L. B. Steren, Exchange-bias effect at $La_{0.75}Sr_{0.25}MnO_3/LaNiO_3$ interfaces, Phys. Rev. B **85**, 094427 (2012).

[31] M. Kitamura, K. Horiba, M. Kobayashi, E. Sakai, M. Minohara, T. Mitsuhashi, A. Fujimori, T. Nagai, H. Fujioka, and H. Kumigashira, Spatial distribution of transferred charges across the heterointerface between perovskite transition metal oxides $LaNiO_3$ and $LaMnO_3$, Appl. Phys. Lett. **108**, 111603 (2016).

[32] M. Medarde, A. Fontaine, J. L. García-Muñoz, J. Rodríguez-Carvajal, M. De Santis, M. Sacchi, G. Rossi, and P. Lacorre, RNiO$_3$ perovskites (R=Pr,Nd): Nickel valence and the metal-insulator transition investigated by x-ray-absorption spectroscopy, Phys. Rev. B **46**, 14975 (1992).

[33] R. Aso, D. Kan, Y. Shimakawa, and H. Kurata, Atomic level observation of octahedral distortions at the perovskite oxide heterointerface, Sci. Rep. **3**, 2214 (2013).

[34] D. Kan, M. Anada, Y. Wakabayashi, H. Tajiri, and Y. Shimakawa, Oxygen octahedral distortions in the compressively strained $SrRuO_3$ epitaxial thin films, J. Appl. Phys. **123**, 235303 (2018).

[35] H. D. Nguyen and Y. Morikawa (private communication).

[36] L. Qiao and X. Bi, Direct observation of Ni^{3+} and Ni^{2+} in correlated $LaNiO_{3-\delta}$ films, Europhys. Lett. **93**, 57002 (2011).

[37] N. Parragh, G. Sangiovanni, P. Hansmann, S. Hummel, K. Held, and A. Toschi, Effective crystal field and Fermi surface topology: A comparison of d- and dp-orbital models, Phys. Rev. B **88**, 195116 (2013).

[38] J. A. Alonso, J. L. García-Muñoz, M. T. Fernández-Díaz, M. A. G. Aranda, M. J. Martínez-Lope, and M. T. Casais, Charge Disproportionation in RNiO$_3$ Perovskites: Simultaneous Metal-Insulator and Structural Transition in $YNiO_3$, Phys. Rev. Lett. **82**, 3871 (1999).

[39] J. A. Alonso, M. J. Martínez-Lope, M. T. Casais, J. L. García-Muñoz, and M. T. Fernández-Díaz, Room-temperature monoclinic distortion due to charge disproportionation in RNiO$_3$ perovskites with small rare-earth cations (R = Ho, Y, Er, Tm, Yb, and Lu): A neutron diffraction study, Phys. Rev. B **61**, 1756 (2000).

[40] M. Medarde, M. T. Fernández-Díaz, and Ph. Lacorre, Long-range charge order in the low-temperature insulating phase of $PrNiO_3$, Phys. Rev. B **78**, 212101 (2008).

[41] D. D. Sarma, Electronic structure of transition metal compounds: Photoemission experiments and model hamiltonian calculations, J. Solid State Chem. **88**, 45 (1990).

[42] J.-S. Zhou and J. B. Goodenough, Chemical bonding and electronic structure of RNiO$_3$ (R=rare earth), Phys. Rev. B **69**, 153105 (2004).